A Complete Energy Budget using a Local Available Potential Energy Density

M. Jeroen Molemaker and James C. McWilliams
IGPP, UCLA

(Received 7 February 2008)

Gravitational available potential energy is a central concept in an energy analysis of flows where buoyancy effects are dynamically important. These include, but are not limited to, most geophysical flows with persistently stable density stratification. The volume-integrated available potential energy $\mathcal{E}_{ap}$ is defined as the difference in the actual gravitational potential energy of the system from the reference potential energy for a state with the lowest potential energy that can be reached by adiabatic material rearrangement. $\mathcal{E}_{ap}$ determines how much energy is available for conservative dynamical exchange with kinetic energy. In this paper we introduce new techniques for computing the local available potential energy density E_{ap} in numerical simulations that allow for a more accurate and complete analysis of the available potential energy and its dynamical balances as part of the complete energy cycle of a flow. The definition of E_{ap} permits us to make a spectral decomposition of its dynamical balance with horizontal wavenumber. Several examples illustrate the structure of E_{ap} and its evolution. The greatest attention is given to a simulation of an Eady flow in turbulent equilibrium, where E_{ap} exhibits a vigorous forward energy cascade through the submesoscale range with inertial-range behavior.

1. Introduction

Lorenz (1955) formalized the concept of available potential energy (APE), which has proved to be very useful in energetic analyses of the atmospheric and oceanic general circulations as the appropriate companion to kinetic energy (Lorenz 1967; Huang 1998). APE has also been shown to be a useful quantity for smaller-scale stratified flows (Winters *et al.* 1995).

For an incompressible fluid the domain integrated APE $\mathcal{E}_{ap}$ is easily defined as the difference between the total potential energy $\mathcal{E}_p$ and the potential energy of a reference state $\mathcal{E}_p^*$,

$$\mathcal{E}_{ap} \;=\; -\int\int\int z\;(b-b^*)\,dx\;dy\;dz\,, \tag{1.1}$$

where g is the gravitational acceleration acting downward in the vertical direction $\hat{\mathbf{z}}$ and $b = g(\rho/\rho_0 - 1)$ is the buoyancy field proportional to the potential density ρ that is conserved on fluid parcels in the absence of diffusion or interior heating or material sources. (ρ_0 is a background constant value.) $b^*(z)$ is the reference buoyancy profile that corresponds to the lowest amount of potential energy that can be reached be adiabatic rearrangement of parcels within a bounded domain. To evaluate $\mathcal{E}_{ap}$ it is, off course, necessary to evaluate $b^*(z)$, a global property of $b(x, y, z)$. The unavailable potential

energy is defined by the residual,

$$\mathcal{E}_{up} \;=\; \mathcal{E}_p - \mathcal{E}_{ap}. \tag{1.2}$$

A stably stratified, resting state has $\mathcal{E}_{ap} = 0$ and $\mathcal{E}_{up} = \mathcal{E}_p = \mathcal{E}_p^*$.

In analogy with — and in dynamical exchanges with (Sec. 3) — the local kinetic energy density, $E_k = \mathbf{u}^2/2 \geq 0$, we are interested in identifying a local APE density, $E_{ap} \geq 0$, that is integrally consistent with (1.1),

$$\mathcal{E}_{ap} \;=\; \int\int\int E_{ap}\, dx\; dy\; dz\,. \tag{1.3}$$

The integrand in (1.1) is not an acceptable local APE density because it is not sign-definite and does not have an obvious spectral expression analogous to that for kinetic energy.

The dynamical approximations of a small-amplitude gravity wave linearized about a stably stratified, resting state and a quasigeostrophic asymptotic approximation, where buoyancy fluctuations are assumed weak compared to the background stratification, both have an energy conservation principle with a local potential energy density that satisfies our requirements for APE density, *viz.,*

$$E_{ap} \;=\; \frac{1}{2}\,\frac{(b-b^*)^2}{N^2} \;\geq\; 0\,. \tag{1.4}$$

Here $N^2 = \partial_z b^* \geq 0$ is the squared buoyancy frequency and $b^*(z)$ is identified with the resting-state stable stratification (Pedlosky 1987). However, we are also interested in more general dynamical regimes with large-amplitude differences between b and b^*, including flows that are unstably stratified. Several valid formulas for E_{ap} have been proposed (Holliday and McIntyre 1981; Henyey 1983; Shepherd 1993); all of these formulas require a determination of $b^*(z)$. An alternative approach was suggested in Tseng and Ferziger (2001), where a probability density function of b is used to approximate b^*.

A special case is the situation where the reference-state stratification profile b^* is linear in z (*i.e.,* constant $N = N_o$). Then (1.4) is a correct APE even for finite amplitude $b - b^*$ (*e.g.,* Lindborg (2006)). However, the formula used in Lindborg (2006),

$$E_{ap_o} = \frac{1}{2}\,\frac{(b-N_o^2 z)^2}{N_o^2}, \tag{1.5}$$

is not a correct APE for a general $b^*(z) \neq N_o^2 z$, because in the limit of small fluctuations it is not quadratic in fluctuation amplitude (Shepherd 1993).

2. Estimation of the Reference State

For most geophysical applications the technique proposed in Winters *et al.* (1995) is used for determining b^* in numerical simulation models. They suggest that a numerical sorting algorithm can be employed to rearrange density values with the densest fluid assigned to the available grid-boxes that have the lowest vertical coordinate. This recipe allows for computation of the reference state potential energy density $E_p^* = -\,z\; b^*$, and therefore $\mathcal{E}_{ap}$, using (1.1).

In Molemaker *et al.* (2007) a small modification to the sorting procedure was introduced that allows for a more accurate determination of E_p^*. After sorting in three dimensions (3D) among the finite number of model grid-boxes as in Winters *et al.* (1995), the resulting buoyancy field b_s is characterized by small departures from a horizontally uniform profile. This means that even though the potential energy $\mathcal{E}_{ps}$ of the sorted field is the

lowest $\mathcal{E}_p$ that can be reached for a given grid resolution there is still some potential energy available for exchange with $\mathcal{E}_k$. However, we can assume that these departures are small relative to the vertical stratification of both the sorted and uniform states. In fact, the departures are guaranteed to be smaller than the difference in density between the successive vertical levels. For this sorted 3D field the linearized definition of APE (1.4) is quite accurate. We therefore propose that the APE of the sorted buoyancy field be evaluated using

$$E_{aps} = \frac{(b_s - \overline{b}_s)^2}{2\partial_z \overline{b}_s}\,, \tag{2.1}$$

with the overbar defined as a horizontal average. The APE of the actual buoyancy field can now be calculated by the amended formula,

$$\mathcal{E}_{ap} = \mathcal{E}_p - \mathcal{E}_{ps} + \mathcal{E}_{aps}\,, \tag{2.2}$$

where $\mathcal{E}_{ps}$ is the potential energy of $\overline{b}_s$ and $\mathcal{E}_{aps}$ is the integral of (2.1). In discrete computations we approximate b^* by $\overline{b}_s$, which is 2nd-order accurate in spatial resolution (Sec. 5.1).

3. APE Density and Its Dynamical Equation

Consider $\mathcal{Z}[b]$, the inverse function defined by the basic state stratification $b^*(z)$. In Holliday and McIntyre (1981) a local definition of E_{ap} is introduced that is suitable for a model in which b is a dependent variable and z is an independent one (such as the ones we use in Sec. 5):

$$E_{ap}(x,y,z) \;=\; \int_{\overline{b}_s(z)}^{b(x,y,z)} \Big(\mathcal{Z}[\tilde{b}] - \mathcal{Z}[b^*]\Big)\; d\tilde{b} \;\geq\; 0\,. \tag{3.1}$$

Since E_{ap} is an explicit function of b alone (albeit implicitly a function of (x,y,z)), we can evaluate a local budget for E_{ap} using the various terms in the discretized buoyancy equation in combination with additional finite-difference approximations†. If b is governed by an advection diffusion equation, we can formally write the local APE evolution equation as

$$\frac{\partial E_{ap}}{\partial t} \;=\; Adv[E_{ap}] + Dif[E_{ap}]\,, \tag{3.2}$$

where Adv and Dif are the local advection and diffusion operators, respectively. These operators are evaluated by finite-differences, *e.g.,*

$$Adv[E_{ap}] \;=\; \frac{E_{ap}[b - \delta\ \mathbf{u}\cdot\nabla b] - E_{ap}[b]}{\delta}\,. \tag{3.3}$$

Here, $(-\,\mathbf{u}\cdot\boldsymbol{\nabla} b)$ is the local buoyancy advective-tendency operator as it is evaluated in the numerical model. δ is chosen to be small but large enough to avoid numerical rounding errors. Also,

$$Dif[E_{ap}] \;=\; \frac{E_{ap}[b + \delta\ \nabla^2 b] - E_{ap}[b]}{\delta}\,, \tag{3.4}$$

where $\nabla^2 b$ is the diffusion operator and μ is the buoyancy diffusivity. Using these difference approximations we can evaluate (3.2) at each point in the domain and analyze the energetic consequences of different terms in the buoyancy equation. A spatial integration of $Adv[E_{ap}]$ and $Dif[E_{ap}]$ over the whole domain will lead to a global budget for

† This approach is an extension of the energy evolution equation (3.9) in Shepherd (1993).

$\mathcal{E}_{ap}$ and, in particular, allow the evaluation of the wavenumber transfer function (*i.e.,* APE cascade); energy conversions with $\mathcal{E}_k$ and $\mathcal{E}_{up}$; dissipation rate for APE; and APE boundary fluxes, if any.

4. Spectral Analysis of the APE Balance

In the context of low-frequency, large-scale oceanic circulation, we are particularly interested in the dynamical routes toward energy dissipation, both kinetic and potential (Muller *et al.* 2005; Molemaker *et al.* 2007). For this we require a spectral analysis of (3.2). In its present form the equation is not suited for spectral analysis, since such analysis requires the computation of co-spectra. However, since E_{ap} is positive semi-definite and has units [m^2 s^{-2}] of a quadratic quantity, we introduce a new quantity $\mathcal{A}$ with units of [m s^{-1}] that is analogous to the role played by $\mathbf{u}$ in $E_k = \mathbf{u}^2/2$:

$$E_{ap} \;=\; \frac{1}{2}\,\mathcal{A}^2\,. \tag{4.1}$$

We propose that $\mathcal{A}$ be called the gravitional deformation function since it is relate to the amount of gravitational energy that is contained in the spatial deformation of the density field relative to its reference state b^* (loosely analogous to the definition of elastic potential energy). In a small-fluctuation limit, E_{ap} can be found using (2.1), so that $\mathcal{A} \rightarrow (b - b^*)/N$. More generally, we propose that $\mathcal{A}$ be defined by

$$\mathcal{A} = sgn[b - b^*]\,\sqrt{2E_{ap}}\,. \tag{4.2}$$

With this definition we can rewrite (3.2) as

$$\mathcal{A}\frac{\partial \mathcal{A}}{\partial t} = \mathcal{A}\;Adv[\mathcal{A}] + \mathcal{A}\;Dif[\mathcal{A}]\,, \tag{4.3}$$

where $Adv[\mathcal{A}]$ and $Dif[\mathcal{A}]$ are obtained analogous to (3.3) and (3.4).

An APE spectrum is now obtained as the power spectrum of $\mathcal{A}$:

$$E_{ap}(k) = \frac{1}{2}\,\hat{\mathcal{A}}(k)^+\,\hat{\mathcal{A}}(k)\,, \tag{4.4}$$

with $\hat{\mathcal{A}}(k)$ the Fourier transformation of $\mathcal{A}(x, y, z)$ and superscript $^+$ the complex conjugate. Spectral versions of the different terms in the energy balance (4.3) are analogously obtained using co-spectra of $\hat{\mathcal{A}}(k)$ and the transformed right-side terms.

5. Illustrations

In this section we present three examples of the structure and evolutionary behavior of E_{ap} and its dynamical balance. The first example is a tilted, stratified buoyancy field that spins down to a resting state. This example is used to compute $\mathcal{E}_{ap}$ in several different ways to assess their accuracy. The second example is an unstable stratification that evolves passively in a specified overturning circulation. The third example is an application of our proposed APE methodology to complete the equilibrium energy balance of a turbulent Eady flow that is examined in Molemaker *et al.* (2007).

5.1. *Spin-Down of a Tilted Buoyancy Gradient*

Consider the following non-rotating fluid system:

$$\begin{aligned} \partial_t \mathbf{u} &= -\boldsymbol{\nabla}\phi + \hat{\mathbf{z}}b + \nabla^2\mathbf{u} \\ \boldsymbol{\nabla}\cdot\mathbf{u} &= 0 \end{aligned}$$

$$\partial_t b = -\boldsymbol{\nabla} \cdot (\mathbf{u} b)\,, \tag{5.1a}$$

where $\mathbf{u}$ is a velocity vector (u, v, w), b is the buoyancy, and ϕ is the normalized pressure p/ρ_0. The domain is $x \in [0,1] \times y \in [0,1] \times z \in [0,1]$, and the boundary conditions are no normal flow and no flux of momentum. This system is adiabatic since the buoyancy equation does not include a diffusive term. We define initial values for the fields $(\mathbf{u}, b, \phi)$ with $\mathbf{u} = 0$, $b(x, y, z) \neq 0$ a tilted, stably stratified buoyancy field, and ϕ in hydrostatic balance with b. Starting from this motionless state, the evolution develops motion in the (x, z) plane and a nonzero value for $\mathcal{E}_k$ by conversion (release) of potential energy. The $\mathcal{E}_k$ is subsequently dissipated by viscous diffusion. The end-state of this evolution returns to a resting state again as $t \to \infty$, where the buoyancy field corresponds to b_s, the state with the lowest potential energy that can be reached adiabatically using this model configuration.

As a test case we consider an initial buoyancy field with a uniform, tilted spatial gradient:

$$b(x, y, z, 0) \;=\; \gamma(z - 0.5) + \alpha(x - 0.5)\,. \tag{5.2}$$

If $|\alpha| < \gamma$, the stratification is gravitationally stable everywhere. $\alpha \ll \gamma$ is the weak-fluctuation limit.

Given the system (5.1), the potential energy $\mathcal{E}_p$ is calculated analytically to be

$$\mathcal{E}_p \;=\; -\int\int\int z\; b\; db \;=\; \gamma \left(\frac{1}{3} z^3 - \frac{1}{4} z^2 \right) \Big|_0^1 \;=\; \frac{1}{12}\gamma\,, \tag{5.3}$$

and the APE can be calculated with simple though tedious calculus:

$$\mathcal{E}_{ap} \;=\; \frac{\alpha^2}{24\gamma} - \frac{\alpha^3}{120\gamma^2}\,. \tag{5.4}$$

This reduces to the weak-fluctuation expression $E_{ap} = \alpha^2/24\gamma$ for $\alpha << \gamma$.

In Fig. 1 E_{ap} is shown for different values of α for a configuration with a $16 \times 16 \times 16$ grid. This may seem like a very course grid resolution, but the use of relatively few vertical levels is common in atmospheric and oceanic modeling.

Figure 2 shows the results of the time integration with a discretized form of the set of equations (5.1). A second-order, central-difference scheme is used to advect the buoyancy field since it is strictly non-dissipative. Dissipative errors are minimized by using a 2nd-order Adams-Bashford time-stepping algorithm with very small time-steps. The system is integrated in time until a resting state occurs. The left panel of Fig. 2 shows the evolution of $\mathcal{E}_p$ as a function of time. Initially the system is at rest. For $t > 0$, $\mathcal{E}_{ap}$ is converted into $\mathcal{E}_k$, which is subsequently dissipated by viscosity. When the $\mathcal{E}_p$ of the system is in the lowest possible state, there is no more $\mathcal{E}_p$ available for conversion, and the system returns to rest. The $\mathcal{E}_{ap}$ of the original state is equal to the difference between the E_p values in initial and the final states. Oscillations in the evolution of $\mathcal{E}_p$ signify back and forth exchanges between kinetic and potential energy. The right panel of Fig. 2 is a copy of the right in Fig. 1 with late-time integration results added (asteriks). Notice that the newly proposed discrete methods (red and green lines) are better predictors of the discrete APE than the analytically computed value. The new methods are also more accurate approximations for the analytic value than are the alternative discrete methods examined here.

In this adiabatic example there is no exchange between $\mathcal{E}_{ap}$ and $\mathcal{E}_{up}$. Initially the total potential energy of the buoyancy field is $\mathcal{E}_p = \mathcal{E}_{up} + \mathcal{E}_{ap}$. For $t \to \infty$ all $\mathcal{E}_{ap}$ has been converted into kinetic energy and subsequently dissipated, reducing $\mathcal{E}_p$ by exactly that amount. Therefore, throughout the evolution $\mathcal{E}_{up}$ is constant.

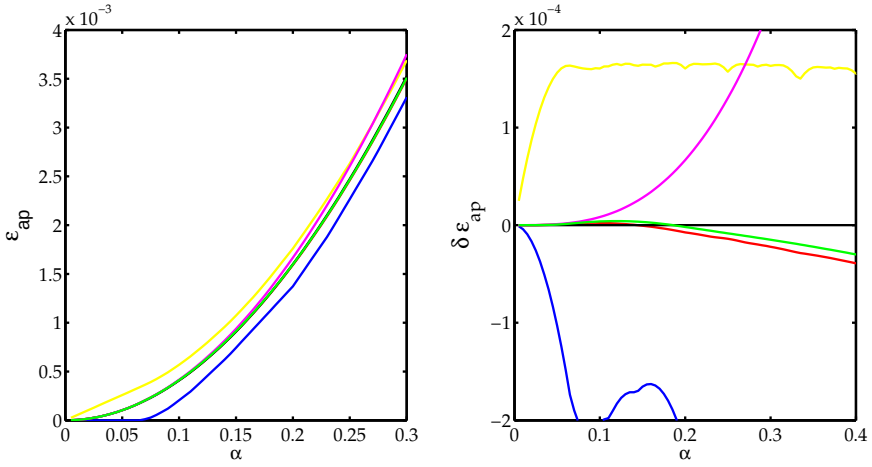

FIGURE 1. $\mathcal{E}_{ap}$ for the tilted stratification example for a range of α values. The left panel includes the analytically computed value (black) (5.4); the analytic weak-fluctuation value (magenta) (1.4); the value found by sorting on the model grid (yellow); the value found by redistribution and computation of $\mathcal{E}_{ps}$ with a much finer vertical grid (blue); the amended sorting technique (2.2) (red); and the domain integral of the local definition of E_{ap}, (3.1) (green). The right panel re-plots the same curves as differences $\delta\mathcal{E}_{ap}$ from the analytically computed $\mathcal{E}_{ap}$; the new discrete techniques (red and green lines) are the most accurate and are nearly indistinguishable from each other.

TABLE 1. Discrete convergence behavior for the error in $\mathcal{E}_{ap}$ as a function of spatial resolution for different definitions of $\mathcal{E}_{ap}$ in the tilted stratification example with $\alpha = 0.4$ and $\gamma = 1$. The truth standard is the analytic value $\mathcal{E}_{ap} = 6.133e-3$, and the error for the weak-fluctuation definition (1.4) analytic value is $\mathcal{E} = 0.533e-3$. The recommended new techniques are in the last two columns.

Resolution	Sorting	Fine Sorting	Amended Sort (2.2)	Local Definition (3.1)
16×16	$0.2526\text{x}10^{-3}$	$-0.1554\text{x}10^{-3}$	$0.0391\text{x}10^{-3}$	$0.0300\text{x}10^{-3}$
32×32	$0.0666\text{x}10^{-3}$	$-0.0390\text{x}10^{-3}$	$0.0117\text{x}10^{-3}$	$0.0100\text{x}10^{-3}$
64×64	$0.0174\text{x}10^{-3}$	$-0.0098\text{x}10^{-3}$	$0.0033\text{x}10^{-3}$	$0.0030\text{x}10^{-3}$
128×128	$0.0044\text{x}10^{-3}$	$-0.0024\text{x}10^{-3}$	$0.0009\text{x}10^{-3}$	$0.0008\text{x}10^{-3}$
256×256	$0.0011\text{x}10^{-3}$	$-0.0006\text{x}10^{-3}$	$0.0002\text{x}10^{-3}$	$0.0002\text{x}10^{-3}$

5.2. *APE Evolution in an Overturning Flow*

In this section we present an example to illustrate the local quantities in the new algorithm for E_{ap} and its evolution. Consider the unstably stratified initial buoyancy field,

$$b(x, y, z, 0) \;=\; 1 - z\,, \tag{5.5}$$

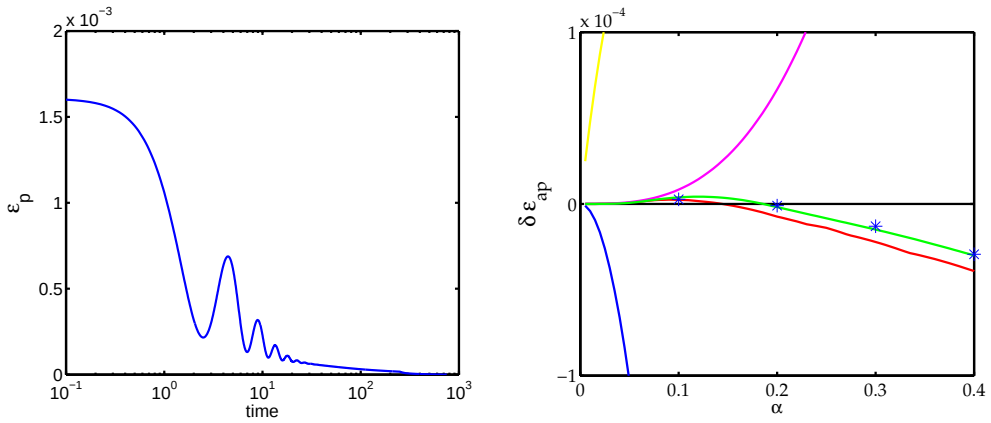

FIGURE 2. Spin-down of the tilted stratification in (5.2). The left panel shows the potential energy relative to the final value as a function of time until the system is at rest. The difference between initial and final $\mathcal{E}_p$ values is the discrete $\mathcal{E}_{ap}$. The right panel here is a blow-up of the right panel in Fig. 1 but adding the results of the time integration of the discrete system as blue $*$ symbols in comparison to the initial-state estimates of $\delta\mathcal{E}_{ap}$.

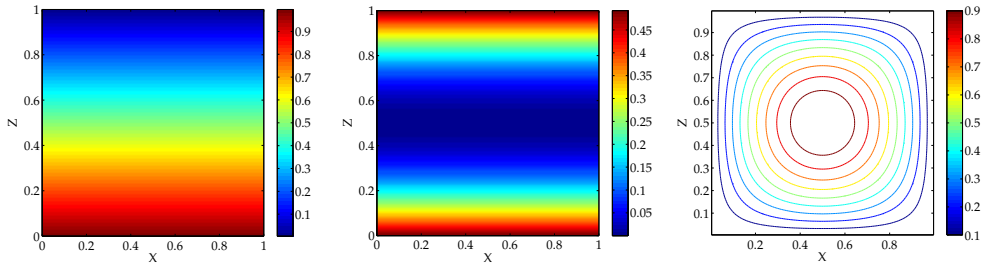

FIGURE 3. Initial state for b, E_{ap}, and Ψ for the stratified overturning example.

for a two-dimensional domain ($x \in [0,1]$, $z \in [0,1]$) with no buoyancy flux through the boundary. This buoyancy field evolves by the advection-diffusion equation,

$$\frac{\partial b}{\partial t} = -\,\mathbf{u}\cdot\boldsymbol{\nabla} b + \mu\nabla^2 b\,, \tag{5.6}$$

where the two-dimensional velocity $\mathbf{u} = (u, 0, w)$ is prescribed as constant in time with $u = -\partial_z\Psi$, $w = \partial_x\Psi$, and streamfunction,

$$\Psi(x,z) \;=\; \sin[\pi x]\,\sin[\pi z]\,. \tag{5.7}$$

The diffusion coefficient is set to the relatively small value of $\mu = 2\times 10^{-3}$, and no-flux buoyancy conditions are prescribed at all boundaries. Figure 3 shows the initial b, APE density, and Ψ fields. E_{ap} has its maximum values near upper and lower boundary indicating the largest difference between the local b and b^*.

The model (5.6) is integrated in time to a fraction of the turnover time for the circulation, $t = 0.5$. The resulting fields of b, E_{ap}, and $\mathcal{A}$ are shown in Fig. 4. The buoyancy field is being swept around by the circulation. As a result of advection by the constant velocity field, some of the higher buoyancy values have been transported upwards and lower ones downward, reducing both $\mathcal{E}_p$ and $\mathcal{E}_{ap}$. In addition to a reduction of $\mathcal{E}_{ap}$ in the integral sense, the E_{ap} field has been rearranged as well. The right panel in Fig. 4 shows

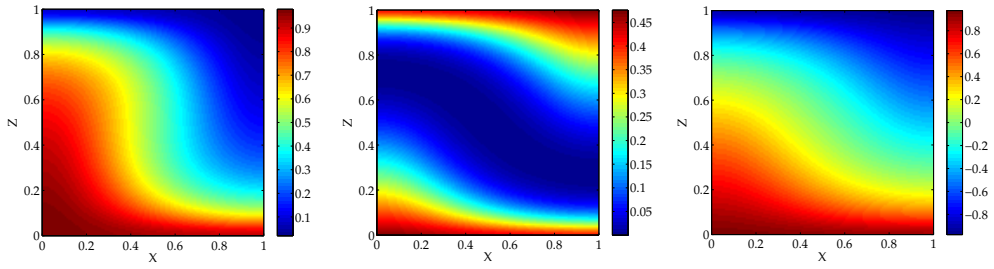

FIGURE 4. Fields of b (left panel), E_{ap} (middle panel), and $\mathcal{A}$ (right panel) at $t = 0.5$ for the stratified overturning example (Fig. 3) that evolves through advection and diffusion in (5.6).

the spatial distribution of $\mathcal{A}$. While bearing gross similarities to b, the field of $\mathcal{A}$ in (4.2) is significantly different in its details, consistent with the definition of E_{ap} in (3.1).

Figure 5 shows the E_{ap} tendency patterns that result from the advection of b in (5.6) in the unstably stratified example. The upper-left panel shows advection of b, heating the upper-left corner of the domain and cooling the lower-right corner, and thus reducing E_{ap} overall. The upper-right panel shows the effect of $\mathbf{u} \cdot \boldsymbol{\nabla} b$ on the distribution of E_{ap}. This pattern is not a pure redistribution of E_{ap} because it reflects the reduction of $\mathcal{E}_{ap}$. However, it can be shown that this pattern is the result of a combination of $\mathbf{u} \cdot \boldsymbol{\nabla} E_{ap}$, a pure spatial redistribution of energy and $w\ (b - b_s)$, a conversion of E_{ap} into E_k. The lower two panels in Fig. 5 illustrate this concept with $Adv[E_{ap}]$ and $\mathbf{u} \cdot \boldsymbol{\nabla} E_{ap}$. This solidifies our notion that E_{ap} is not a purely artificial construct but in fact has physical significance.

Shifting attention to the gravitational deformation function $\mathcal{A}$, the upper row of Fig. 6 compares the advection of b: $-\mathbf{u} \cdot \nabla b$ with $Adv[\mathcal{A}]$, demonstrating their close correspondence for this case. Unlike the relation between $adv[E_{ap}]$, $w(b - b_s)$ and $-\mathbf{u} \cdot \nabla E_{ap}$, this correspondence is not exact in all cases. The lower row of Fig. 6 shows $w(b - b_s)/f$ and $-\mathbf{u} \cdot \nabla \mathcal{A}$, which added together lead to the pattern of $Adv[\mathcal{A}]$.

Examination of the results reveals that

$$Adv[E_{ap}] + w(b - b_s) \;=\; -\,\mathbf{u} \cdot \nabla E_{ap} \tag{5.8}$$

to within the 2nd-order numerical accuracy of the discretizations used to approximate (3.1). Also, we find that

$$Adv[\mathcal{A}] - w(b - b_s)/\mathcal{A} \;=\; -\,\mathbf{u} \cdot \nabla \mathcal{A}\,, \tag{5.9}$$

which follows from the equivalent relation for the advection of E_{ap} and the definition of $\mathcal{A}$ in (4.2).

Next, the diffusive term in (5.6) and its effect on $\mathcal{A}$ are examined. Again, the evolution of $\mathcal{A}$ as a result of $\nabla^2 b$ appears to be very closely related to $\nabla^2 b$ itself. The effect of diffusion on E_{ap} is given by $\mathcal{A}\ Dif[\mathcal{A}]$, and for this case it is negative when integrated over the domain, dominated by regions of E_{ap} destruction near the upper and lower boundaries.

5.3. *Spectral Energy Balance in an Eady Flow*

Molemaker *et al.* (2007) investigates the turbulent equilibrium state for an unstable, geostrophically-balanced, vertically-sheared horizontal flow with uniform background rotation and stable stratification in a horizontally-periodic, vertically-bounded domain for solutions of the incompressible Boussinesq equations. This is the mean flow analyzed by Eady (1949) for its quasigeostrophic linear baroclinic instability and for more general linear instabilities by Stone (1966) and Molemaker *et al.* (2005).

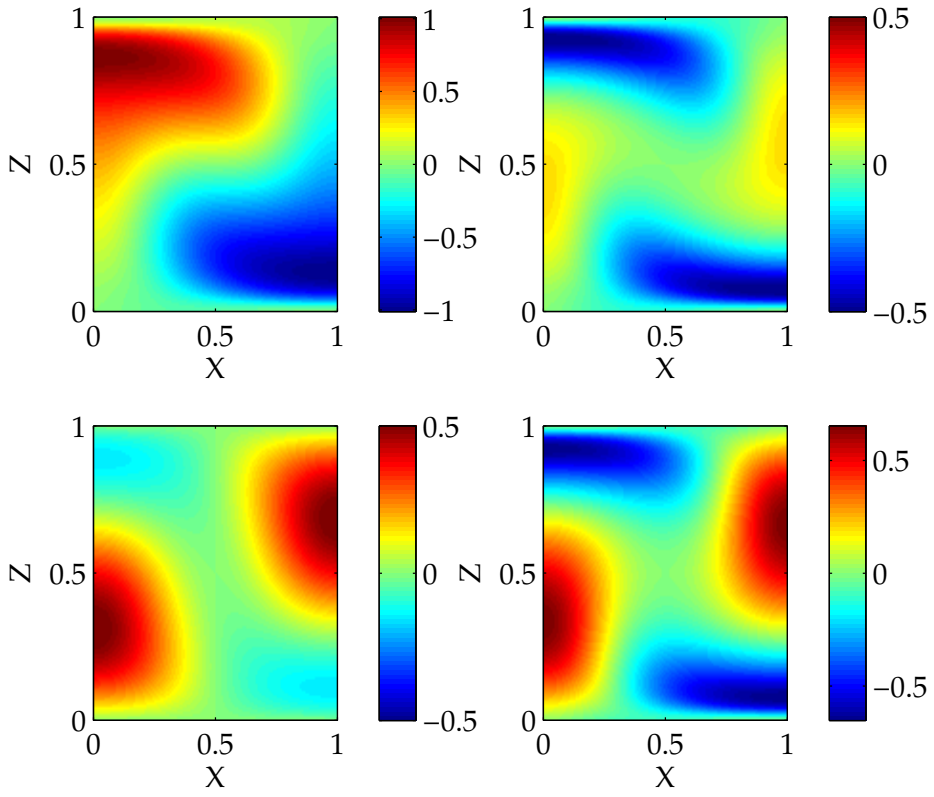

FIGURE 5. Spatial pattern of tendencies that result from the advection of b at $t = 0.5$ for the stratified overturning example in Fig. 3: $-\mathbf{u} \cdot \nabla b$ (upper-left panel); $Adv[E_{ap}]$ (upper-right); $w(b - b_s)$ (lower-left); and $-\mathbf{u} \cdot \nabla E_{ap}$ (lower-right). The advective evolution of E_{ap} is a combination of redistribution of E_{ap} by $\mathbf{u} \cdot \nabla E_{ap}$ and release of potential energy by $w(b - b_s)$.

The fluctuations about the Eady flow during the equilibrium state are a combination of the following:

(a) Geostrophically balanced eddies arising from instability of the "mean" Eady flow, with a horizontal scale near the first baroclinic deformation radius and significant inverse energy cascade toward larger scales (as expected in geostrophic turbulence; Charney (1971)).

(b) Surface-intensified buoyancy fronts, generated through straining by the larger eddies, that induce significant buoyancy restratification and generate E_k on intermediate scales by $\overline{w'b'} > 0$ conversion, with strong local deviations from geostrophic, hydrostatic balance.

(c) Similarly unbalanced,horizontal-shear instabilities of the fronts that arrest the frontogenesis at an intermediate scale and further advance the forward kinetic-energy cascade toward small-scale dissipation.

In the previous investigation (Molemaker *et al.* 2007), particular emphasis was given to the energy budget in the turbulent-equilibrium state and the dynamical route to small-scale, viscous dissipation of kinetic energy. Using the the modification of the sorting procedure by Winters *et al.* (1995) described in Sec. 2, it was possible to include a

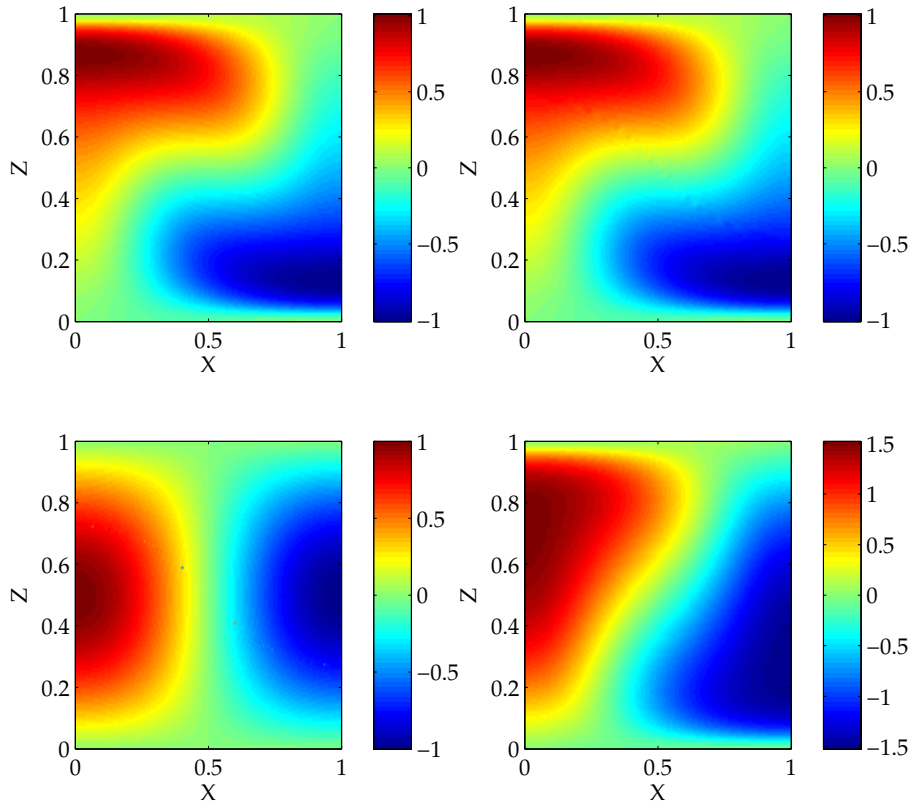

FIGURE 6. Spatial pattern of tendencies that result from the advection of b at $t = 0.5$ for the initially unstably stratified example. $-\mathbf{u}\cdot\boldsymbol{\nabla}b$ (upper-left panel), $Adv[\mathcal{A}]$ (upper-right panel), $-w(b-b_s)/\mathcal{A}$ (lower left panel) and $-\mathbf{u}\cdot\boldsymbol{\nabla}\mathcal{A}$ (lower right). The effect of advection on $\mathcal{A}$; $Adv[\mathcal{A}]$ is the sum of $w(b-b_s)/\mathcal{A}$ and $-\mathbf{u}\cdot\boldsymbol{\nabla}\mathcal{A}$ to within the overall 2nd-order accuracy of the discretizations.

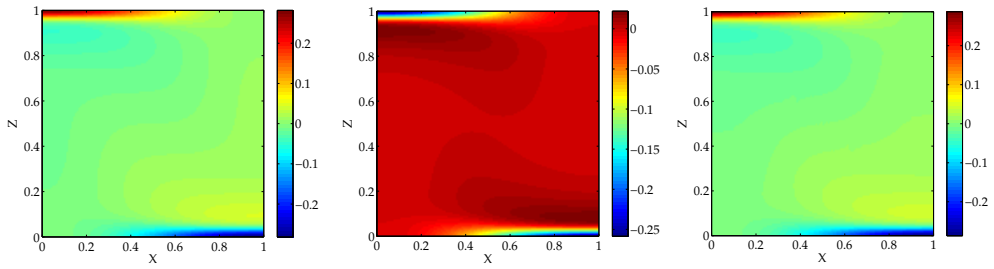

FIGURE 7. Spatial pattern of tendencies that result from the diffusion of b at $t = 0.5$ for the stratified overturning example in Fig. 3: $\mu\nabla^2 b$ (left panel), $Dif[E_{ap}]$ (middle panel), and $Dif[\mathcal{A}]$ (right panel).

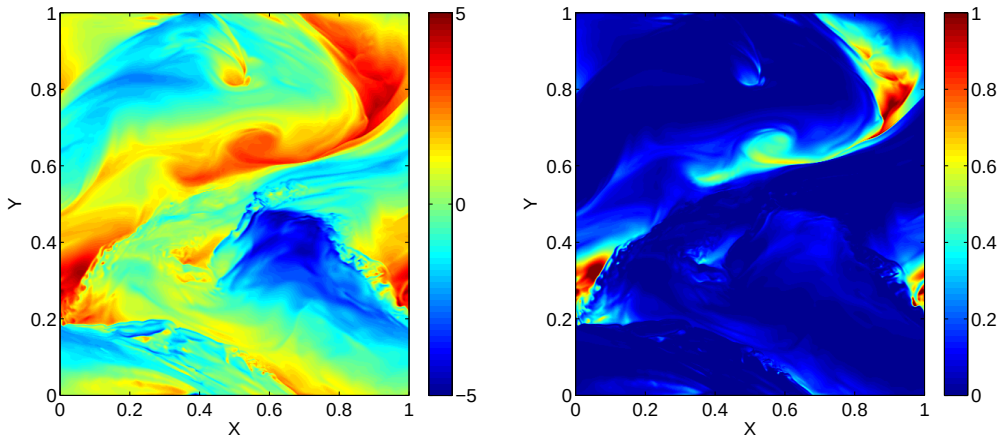

FIGURE 8. Instantaneous horizontal slices at $z = 0.9$ (in a domain with $z \in [0, 1]$) for fluctuation buoyancy (left) and E_{ap} from (3.1) (right) in an equilibrium Eady flow. Both fields are non-dimensional as described in Molemaker *et al.* (2007) for the case with Rossby number $Ro = 0.5$ and Reynolds number $Re = 6600$.

domain-integrated $\mathcal{E}_{ap}$ budget in the energy analysis, along with a detailed spectral decomposition of E_k and its dynamical balance. However, a local E_{ap} that was analogous to E_k was missing. With the formulas in Secs. 3-4, we now can complete this analysis and present a complete view of the total energy as it moves from the mean Eady flow to the fluctuations, from fluctuation APE to kinetic energy, and among different spatial scales in the fluctuation fields.

Figure 8 shows horizontal slices of buoyancy fluctuation and E_{ap}. The eddies are evident on the domain scale. Intermediate-scale buoyancy fronts occur between the eddy centers. Some of the fronts also exhibit fine-scale instabilities. The largest values of E_{ap} are associated with positive buoyancy extrema in this plane near the upper boundary.

Figure 9 shows the horizontal-wavenumber spectra of kinetic energy and APE, averaged in depth and time during the equilibrium phase. For all wavenumbers the amount of E_k is larger than the amount of E_{ap} ($\mathcal{E}_k = 1.40$ and $\mathcal{E}_{ap} = 0.65$), but the spectral slopes are essentially identical. Our provisional interpretation is that the energy ratio is set by the large-scale dynamics, which surely does not exhibit universal behavior. However, the approximate power-law shapes for the intermediate wavenumber range, $K_h \in [20, 80]$, are suggestively close to an energy inertial-range exponent of -5/3. A similar forward-cascade inertial-range in both E_k and E_{ap} is shown in Lindborg (2006) for randomly forced, non-rotating, stratified turbulence (with a uniform background stratification), with approximately the same E_k/E_{ap} ratio as here. This suggests there may be a simple phenomenological continuity in the turbulent cascades as the rotational dynamical control decreases with increasing k, given a sufficiently broad range of resolved scales.

At larger scales (*i.e.,* in the geostrophic and frontogenetic dynamical regimes; Molemaker *et al.* (2007)), as well as in the small-scale dissipation range, the spectrum slopes are steeper. In particular, on scales smaller than the first baroclniic deformation radius, we see a slope consistent with the K_h^{-2} submesoscale frontongenesis regime in Capet *et al.* (2007a), although its wavenumber range is rather short in the Eady problem as posed here. From this perspective we interpret the onset of the $K_h^{-5/3}$ range as at the end of the frontogenesis range where frontal instability becomes dominant.

Figure 10 (top row) the spectral budget of perturbation kinetic energy Ek is shown.

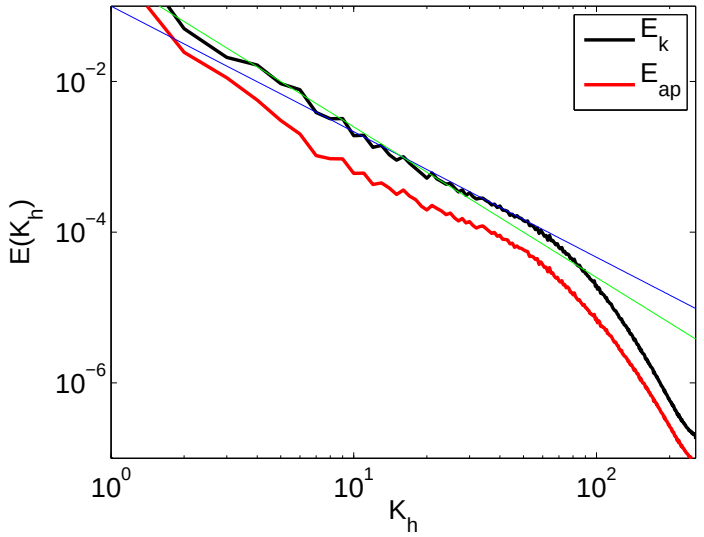

FIGURE 9. Depth-averaged, horizontal-wavenumber spectra for E_{ap} (red) and E_k (black) associated with the fluctuation b and $\mathbf{u}$ fields in an equilibrium Eady flow. The blue (green) line indicates a $k^{-5/3}$ (k^{-2}) dependency.

At low wavenumbers a large transfer of energy from potential to kinetic energy ($\overline{w'b'}$) occurs in association both with the large-scale baroclinic instability of the mean Eady flow and with finer-scale frontogenesis. This energy is transferred in wavenumber space by the nonlinear terms both in an inverse cascade to the lowest available wavenumber ($K_h = 1$ where a linear damping term is active) and to higher wavenumbers *en route* to viscous dissipation. For horizontal wavenumbers greater than $K_h \approx 15$, the release of APE becomes much smaller and the primary energy balance exists between nonlinear energy transfer between wavenumbers and dissipation. Since the dissipation is concentrated at the highest wavenumbers by the model construction, the advective transfer rate is small for the intermediate scales because of approximately constant energy fluxes (5.10) toward the dissipation range. A constant-energy-flux range is commonly referred to as an energy inertial range (Figs. 9 and 11). However, in the expanded amplitude range (Fig. 10, upper-right), we see a weak, reverse energy conversion from E_k to E_{ap} that modifies the simple Kolmogorov conception of a kinetic-energy inertial range†.

The bottom row in Fig. 10 shows the corresponding budget for E_{ap}. It has direct generation by the instability of the mean Eady flow. Energy loss by conversion mirrors the equal-but-opposite effect in the E_k budget: a strong loss in the baroclinic instability and frontogenetic wavenumber ranges and a weak source in the near-inertial range. The advective spectral transfer function for E_{ap} is more extensively positive than it is for E_k. It shows negative values (suggestive of inverse inverse cascade, but also see Fig. 11) at the largest scales, but for somewhat larger wavenumbers the E_{ap} cascade is in a forward direction in association with frontogenesis (*cf.,* Capet *et al.* (2007b)). Again the advective transfer function is small for$K_h > 15$, indicative of nearly constant spectral flux (Fig. 11). Remarkably, the dissipation of E_{ap} appears to be somewhat more scale-selective than that for E_k, in spite of $\mathbf{u}$ and b having equal diffusion coefficients and identical advection

† This reverse conversion from E_k to E_{ap} is reminiscent of the forward energy cascades in stratified turbulence as measured at the microscale in the oceanic interior (Toole 1998).

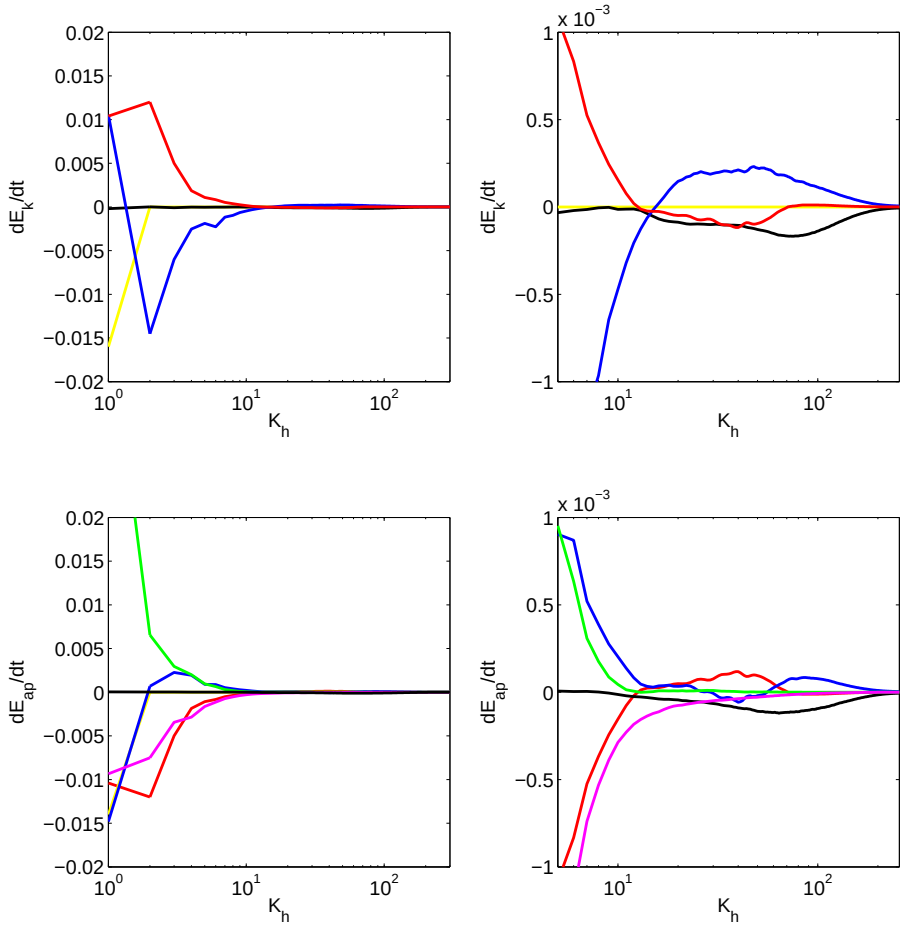

FIGURE 10. Time-averaged, horizontal spectral energy budgets for the fluctuation fields in an equilibrium Eady flow. The right panels show an expanded amplitude range by zooming in on the higher wavenumbers. **Kinetic energy** E_k (top row): release of potential energy $\overline{w'b'}$ (red); transfer function for advective E_k redistribution among wavenumbers (blue); E_k dissipation (black); restoring damping of wavenumber $K_h = 1$ in $\mathbf{u}$ (yellow). **Available potential energy** E_{ap} (bottom row): loss of potential energy by conversion $-\overline{w'b'}$ (red); transfer function for advective E_{ap} redistribution among wavenumbers (blue); E_{ap} dissipation (black); forcing of the fluctuations by instability of the mean Eady flow (green); restoring of buoyancy fluctuations to the basic state stratification (maroon); restoring damping of wavenumber $K_h = 1$ in b (yellow). In both budgets the dissipation is due to a combination of explicit diffusivities and numerical dissipation associated with the 3rd-order, upwind-biased advection scheme.

algorithms. The more restricted dissipation range is reflected in the more nearly constant spectral flux for E_{ap} at intermediate wavenumbers.

An examination of the spectra of the terms in the vertical momentum equation shows that the gravitational force, $\hat{\mathbf{z}}b$ contributes significantly to the fluctuation dynamical balance throughout the energy inertial range up to the onset of the dissipation range. This indicates that the advective forward cascades in kinetic energy and APE are dynamically coupled with each other.

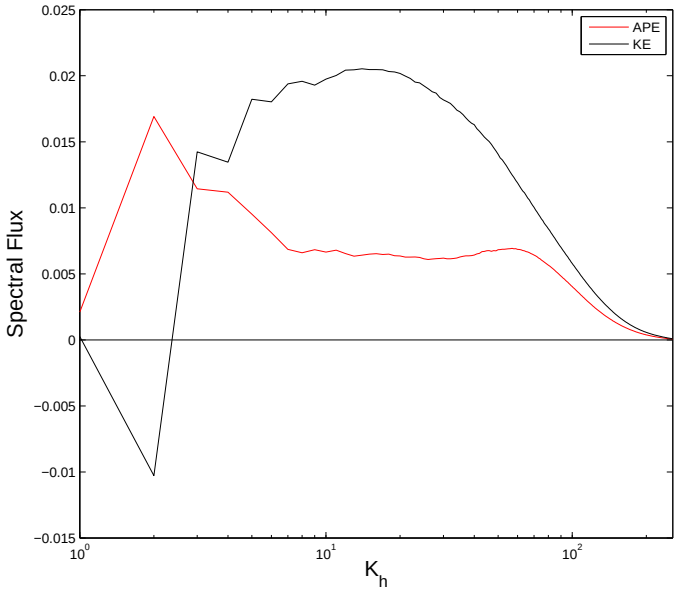

FIGURE 11. Advective spectral fluxes for E_k (black) and E_{ap} (red) with respect to horizontal wavenumber in an equilibrium Eady flow. Positive values indicate forward energy cascades toward larger wavenumber. Note the approximate inertial ranges (*i.e.,* constant flux values) for $K_h \in [7, 70]$, especially for E_{ap}.

The spectral fluxes of energy in Fig. 11 are obtained by integrating the nonlinear redistribution of E_k and E_{ap} in horizontal wavenumber K_h space:

$$\Pi_k(K_h) = \int_0^{K_h} Adv[E_k]\; dK_h$$
$$\Pi_{ap}(K_h) = \int_0^{K_h} (Adv[E_{ap}] + \hat{w}^+\hat{b})\; dK_h\,. \qquad (5.10a)$$

Figure 11 shows well-established forward fluxes for both E_k and E_{ap}, including forward flux even at the domain scale (which might not hold if the domain were much larger than the first baroclinic deformation radius). The absolute amount of forward flux is larger for E_k than for E_{ap}, reflecting the fact that there is more overall $\mathcal{E}_k$ than $\mathcal{E}_{ap}$ in the fluctuations. Consistent with Fig. 10, the forward flux for E_{ap} shows a rather flat curve for Pi, especially between wavenumbers 20 and 50, indicative of an inertial sub-range.

The derivation of a spatially-local, spectrally-decomposable E_{ap} (Secs. 1-4) cannot be extended to E_p, hence not to the residual quantity E_{up}. Nevertheless, all of the forms of potential energy have well-defined integral budgets that we summarize here for completeness. Consistent with the lower row in Fig. 10, the integral budget for $\mathcal{E}_{ap}$ consists of a source by mean flow instability (at a mean rate of +0.15 in the non-dimensional units used in Fig. 6 of Molemaker *et al.* (2007)), balanced by release to kinetic energy (-0.06), mean restratification (-0.06), $k_h = 1$ restoring (-0.02), and diffusive dissipation (-0.01). The integral budget for $\mathcal{E}_p$ is mainly loss by restratification (-0.06) and gain by restoring to the mean buoyancy profile (+0.06), with only a weak source from vertical diffusion (+0.003); it has no direct energy exchange due to the instability of the mean Eady flow. Thus, the integral balance for $\mathcal{E}_{up}$, determined by residual between $\mathcal{E}_p$ and $\mathcal{E}_{ap}$ balances, is

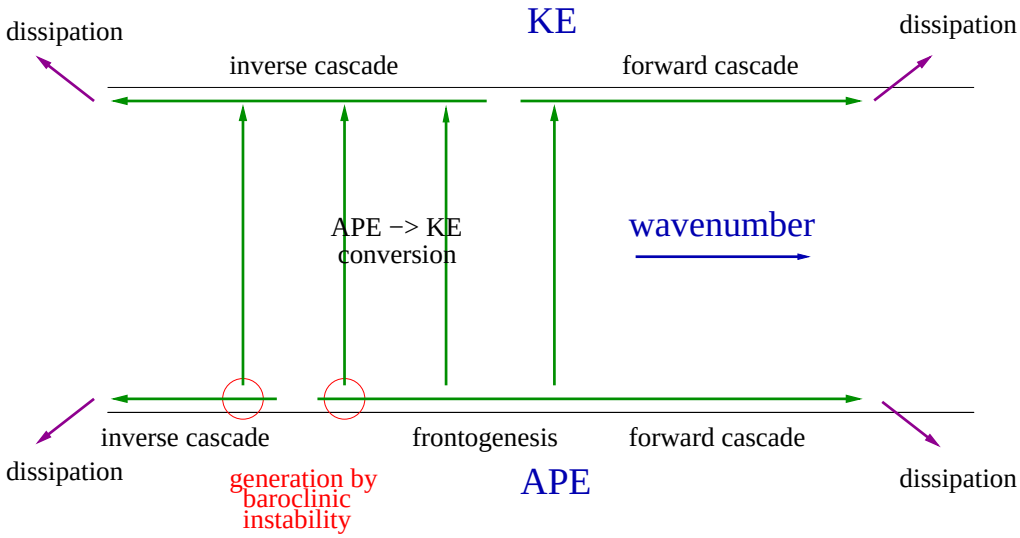

FIGURE 12. Sketch of energy pathways in an equilibrium Eady flow.

gain by restoring (+0.12), loss by mean instability (-0.15), gains by $k_h = 1$ restoring and diffusion (+0.02 and +0.01), and there is no contribution from kinetic energy conversion†.

On the basis of the spectral energy balances (Fig. 10), a summary diagram for the pathways for fluctuation energy from large-scale E_{ap} generation by mean-flow instability to fine-scale diffusive dissipation (and $k_h = 1$ restoring damping) is presented in Fig. 12.

6. Summary

We have introduced two new techniques for calculating gravitational APE energy. The first technique (Sec. 2) is a simple modification of the sorting procedure in Winters *et al.* (1995) that allows for a much more accurate evaluation of the domain-integrated APE in discretized numerical models. It takes advantage of the fact that, while the weak-fluctuation approximation for $\mathcal{E}_{ap}$ in (1.4) may not be accurate for the actual buoyancy field, it is highly accurate for the reference buoyancy field obtained by a 3D sorting procedure. The new technique is both simple to implement and more accurate than all previously suggested methods. It is valid for all regimes that occur in flows with buoyancy effects, including ones with unstable as well as stable stratifications.

The second new technique builds on the local definition of E_{ap} in Holliday and McIntyre (1981). After using the improved sorting procedure to obtain a reference profile of buoyancy, this local definition is used to compute E_{ap} and its dynamical evolution in numerical simulations. With this local definition we define a generalized buoyancy fluctuation as the gravitational deformation field $\mathcal{A}$, which permits us to compute the spectrum of E_{ap}, something that up to now was not possible. Spectral analyses of E_{ap} and its budget make it possible to construct a complete picture of the fluctuation energy budget, both for kinetic and potential components. In an equilibrium Eady flow on scales smaller than the primary energy generation by instability of the mean circulation, there is an energy conversion from E_{ap} to E_k associated with frontogenesis down to a scale set

† For comparison, the $\mathcal{E}_k$ budget in Fig. 6 of Molemaker *et al.* (2007) is gain by release of potential energy (+0.057) and losses by $k_h = 1$ restoring and fine-scale dissipation (-0.03 and -0.03).

by frontal instability, and at even finer cascades there are coupled inertial ranges with forward cascade of both E_{ap} and E_k down to small-scale dissipation. This new technique makes possible the study of energy cascades in both E_k and E_{ap}, opening the way for new analyses and interpretations for all flows with buoyancy effects.

Acknowledgments This research was supported by the National Science Foundation through grants OCE 02-21177, OCE 03-36755, and OCE-0550227.

REFERENCES

Capet, X., McWilliams, J., Molemaker, M., and Shepetkin, A. (2007a). Mesoscale to submesoscale transition in the California Current System: Flow structure and eddy flux. *J. Phys. Ocean.*, in press.

Capet, X., McWilliams, M., Molemaker, M., and Shepetkin, A. (2007b). Mesoscale to submesoscale transition in the California Current System: Frontal processes. *J. Phys. Ocean.*, in press.

Charney, J. (1971). Geostrophic turbulence. *J. Atmos. Sci.*, **28**, 1087–1095.

Eady, E. (1949). Long waves and cyclone waves. *Tellus*, **1**, 33–52.

Henyey, F. S. (1983). Hamiltonian description of stratified fluid dynamics. *Phys. Fluids*, **26**, 40–47.

Holliday, D. and McIntyre, M. (1981). On potential energy density in an incompressible, stratified flow. *J. Fluid Mech.*, **107**, 221–225.

Huang, R. (1998). On available potential energy in a Boussinesq ocean. *J. Phys. Ocean.*, **28**, 669–678.

Lindborg, E. (2006). The energy cascade in a strongly stratified fluid. *jfm*, **550**, 207–242.

Lorenz, E. (1955). Available energy and the maintenance of the general circulation. *Tellus*, **7**, 157–167.

Lorenz, E. (1967). *The Nature and Theory of the General Circulation of the Atmosphere*. World Meteorological Organization.

Molemaker, M., McWilliams, J., and Yavneh, I. (2005). Baroclinic instability and loss of balance. *J. Phys. Ocean.*, **35**, 1505–1517.

Molemaker, M., McWilliams, J., and Capet, X. (2007). Balanced and unbalanced routes to dissipation in equilibrated eady flow. In review for *J. FLuid Mech.*

Muller, P., McWilliams, J., and Molemaker, M. (2005). Routes to dissipation in the ocean: The 2D/3D turbulence conundrum. In H. Baumert, J. Simpson, and J. Sundermann, editors, *Marine Turbulence: Theories, Observations and Models*, pages 397–405. Cambridge Press.

Pedlosky, J. (1987). *Geophysical Fluid Dynamics*. Springer-Verlag.

Shepherd, T. (1993). A unified theory of available potential energy. *Atmosphere-Ocean*, **31**, 1–26.

Stone, P. (1966). On non-geostrophic baroclinic instability. *J. Atmos. Sci.*, **23**, 390–400.

Toole, J. (1998). Turbulent mixing in the ocean. In E. Chassignet and J. Verron, editors, *Oceanic Modeling and Parameterization*, volume C 516, pages 171–189. NATO Science Series, Kluwer Academic Publishers.

Tseng, Y.-H. and Ferziger, J. (2001). Mixing and available potential energy in stratified flows. *Phys. Fluids*, **13**, 1281–1293.

Winters, K., Lombard, P., Riley, J., and D'Asaro, E. (1995). Available potential energy and mixing in density-stratified fluids. *J. Fluid Mech.*, **289**, 115–128.